Radon-222 monitoring at German ICOS atmosphere stations

Maksym Gachkivskyi[1,2], Ute Karstens[3], Bernd Fischer[4], Dagmar Kubistin[5], Jennifer Müller-Williams[5], Matthias Lindauer[5], and Ingeborg Levin[1,†]

[1]Institut für Umweltphysik, Heidelberg University, INF 229, 69120 Heidelberg, Germany
[2]ICOS Central Radiocarbon Laboratory, Heidelberg University, Berliner Straße 53, 69120 Heidelberg, Germany
[3]ICOS ERIC Carbon Portal, Physical Geography and Ecosystem Science, Lund University, Sölvegatan 12, 22362 Lund, Sweden
[4]Umweltbundesamt, Meßstelle Schauinsland, Schauinslandweg 2, 79254 Oberried, Germany
[5]Deutscher Wetterdienst, Meteorological Observatory Hohenpeißenberg, Albin-Schwaiger-Weg 10, 82383 Hohenpeißenberg, Germany
[†]deceased, 10 February 2024

Correspondence: Maksym Gachkivskyi (mgach@iup.uni-heidelberg.de)

Abstract.

Atmospheric measurements of the short-lived radioactive noble gas Radon-222 (^{222}Rn) have many applications. Its concentrations are driven by atmospheric mixing as well as seasonal variations, which follow the seasonality of ^{222}Rn exhalation from continental soils with lower values during the wet winter and spring months compared to more dry summer conditions. Hence, it can be used as tracer to distinguish marine from continental air masses or for transport model validation. The Heidelberg Radon Monitor (HRM) is a static filter detector measuring atmospheric ^{214}Polonium (^{214}Po), which is a progeny of ^{222}Rn. These measurements can be used to infer atmospheric ^{222}Rn activity concentrations if the radioactive disequilibrium between ^{214}Po and ^{222}Rn at the measurement site is known. In this study, ^{214}Po activity concentrations measured with the HRM at 8 stations in the ICOS Germany network are presented, along with guidelines for evaluating these data to estimate atmospheric ^{222}Rn activity concentrations. In addition to the established line-loss and disequilibrium corrections applied when sampling through long tubing or from air intake heights close to the ground, respectively, an upper limit for relative humidity (RH) is suggested, where secular equilibrium can still be assumed. At higher RH, aerosol scavenging effects can cause disequilibrium between ^{214}Po and ^{222}Rn. Using comparison with the model this threshold is determined to be at about 98% RH and was applied uniformly at all measurement sites. A clear diurnal cycle of ^{222}Rn is observed at all German tower stations during the summer and autumn months as well as a seasonal cycle with maximum during summer and autumn months. Overall, our results demonstrate that the ^{214}Po-based ^{222}Rn measurements with the HRM are reliable if the equilibrium conditions between ^{214}Po and ^{222}Rn can be ensured, i.e. for air intake heights above 80-90 m a.g.l. during conditions with RH < 98%. The corrected and ready-to-use dataset of 10-year radon activity concentrations from the 8 ICOS stations is published alongside this paper.

1 Introduction

Radon-222 (^{222}Rn) is a short-lived radioactive noble gas (half-life $T_{1/2}$ = 3.8 days) and it is a progeny of Radium-226 (^{226}Ra), which is a member of the primordial Uranium-238 decay series. It is naturally produced in all soils and as a gas it can escape

from the soil air into the atmosphere. The exhalation rate of ^{222}Rn from continental surfaces depends on the soil properties, such as grain size distribution, porosity and ^{226}Ra content, and it varies with soil moisture and other meteorological parameters (e.g. Nazaroff, 1992; Karstens et al., 2015). The ^{222}Rn flux from (ocean) water surfaces is negligible (Schery and Huang, 2004) compared to that from continental surfaces. Therefore, ^{222}Rn can serve as tracer to distinguish continental from marine air masses (e.g. Dörr et al., 1983; Polian, 1986; Biraud, 2000). While the half-life of radon is short relative to synoptic timescales (approximately 4–12 days), preventing it from accumulating in the atmosphere over longer time scales, it is long compared to mixing timescales in the atmospheric boundary layer (1 hour), allowing it to act as a quasi-conservative tracer for studying boundary layer mixing and transport processes. These properties make ^{222}Rn a suitable tracer for atmospheric boundary layer mixing or transport model validation studies (e.g. Jacob and Prather, 1990; Jacob et al., 1997; Taguchi et al., 2011; Williams et al., 2011) and even for estimation of regional fluxes of other soil-borne trace gases, by applying the Radon-Tracer-Method (e.g. Levin, 1987; Levin et al., 1999, 2021; Grossi et al., 2018), assuming that the spatial and temporal distribution of the ^{222}Rn exhalation rate from continental surfaces is known.

Owing to its applicability as an atmospheric transport tracer, ^{222}Rn observations are recommended as a supplementary measurement component at all ICOS atmosphere stations (ICOS RI, 2020). For precise atmospheric ^{222}Rn observations three fundamentally different measurement principles are available: (1) A two-filter dual flow loop detector developed by ANSTO, Australia (Whittlestone and Zahorowski, 1998; Chambers et al., 2011), (2) an electrostatic deposition monitor developed by INTE-UPC, Spain (Grossi et al., 2016), both measuring ^{222}Rn directly, and (3) static or moving filter detectors, which accumulate ^{222}Rn progeny on a filter and calculate the atmospheric ^{222}Rn activity concentration based on assumptions about the secular equilibrium between ^{222}Rn and its progeny in the atmosphere (e.g. Stockburger and Sittkus, 1966; Polian, 1986; Paatero et al., 1998; Biraud, 2000; Levin et al., 2002; Schmithüsen et al., 2017). This latter ^{222}Rn measurement principle is applied in the static filter system of the Heidelberg Radon Monitor (HRM, Levin et al., 2002), which measures the atmospheric ^{222}Rn progeny ^{214}Po at German ICOS atmosphere stations, and also at sites outside of Germany, including Neumayer station at the Antarctic coast (Weller et al., 2014) and the Amazon Tall Tower Observatory in Brazil (ATTO, Levin et al., 2025).

While the HRM static filter radon monitor is a compact and easy to handle instrument, it has some important caveats, which arise from the fact that ^{222}Rn progeny and not ^{222}Rn itself are measured. In the atmosphere, newly formed ^{222}Rn progeny, such as ^{214}Po, are attached to aerosols and are thus potentially affected by dry or wet deposition processes as well as loss in intake lines if sampling is conducted through long tubing (Levin et al., 2017). Moreover, the state of radioactive equilibrium between progeny and soil-borne ^{222}Rn in the atmosphere depends on the state of atmospheric stability and height above ground (Jacobi and Andre, 1963). There may also be some delay in reaching secular radioactive equilibrium of its progeny after rapid increases of the ^{222}Rn activity concentration. In the past, careful comparison measurements were conducted to evaluate the height-dependence of the disequilibrium (Schmithüsen et al., 2017; Grossi et al., 2020), which turned out to be negligible for measurement heights above ca. 80 m a.g.l. An empirical correction function to compensate for progeny loss in standard 8 mm inner diameter Decabon tubing was determined by extensive laboratory experiments (Levin et al., 2017) and were applied e.g. for the HRM progeny measurements at the German ICOS atmosphere stations to estimate ^{222}Rn activity concentrations from

the measured ^{214}Po data. A remaining uncertainty is the potential progeny loss due to aerosol scavenging and subsequent wet deposition at very high ambient air humidity which have not been investigated in detail yet.

In this paper we present the atmospheric ^{214}Po/^{222}Rn activity concentration data from German ICOS stations spanning eleven years, from 2014 to 2024, and evaluate these data with respect to potential aerosol scavenging effects, depending on ambient air humidity. Such effects are most frequent at sites where the air intake can reach into clouds, i.e. when a tall tower is located on the top of a mountain or hill. We have therefore developed relative humidity (RH) flagging threshold for the HRM that is to be applied to all stations, based on re-evaluation of earlier comparison campaign data as well as preliminary regional transport model estimations of the atmospheric ^{222}Rn activity concentration for the individual sites. The ^{222}Rn data published along with this paper are flagged according to these thresholds.

2 Methods

2.1 Radon progeny observations at German ICOS atmosphere stations

Radon progeny observations with the Heidelberg Radon Monitor (HRM) are conducted at eight ICOS atmosphere stations in Germany. All these ICOS atmosphere stations are operated and managed by the Meteorological Observatory Hohenpeißenberg of the German Meteorological Service (DWD) except for the station Schauinsland (SSL) which is run by the German Environment Agency (Umweltbundesamt, UBA). The stations are listed in Tab. 1 together with their coordinates and intake heights. A map of Germany (Fig. 1) shows their almost even distribution across the country. Except for Schauinsland, a mountain station in the Black Forest (1205 m a.s.l.), where the air intake is about 12 m above ground level (a.g.l.), all other ^{222}Rn progeny measurements are conducted at towers from intake heights between 93 m and 132 m above ground level. The Torfhaus and Hohenpeißenberg towers are located on top of moderately high hills in the Harz (Torfhaus, 801 m a.s.l.) and in the pre-alpine region of Southern Germany (Hohenpeißenberg, 934 m a.s.l.). All other stations are located in flat terrain at altitudes above sea level (a.s.l.) between 29 m and 110 m. Detailed information about all (German) ICOS stations is available at the ICOS Carbon Portal (https://www.icos-cp.eu/observations/atmosphere/stations).

2.2 Measurement principle and correction for aerosol loss in tubing

The HRM accumulates ambient ^{222}Rn progeny on a static filter and measures their alpha decay in situ with a surface barrier detector. Half-hourly alpha spectra are integrated and evaluated to separate the ^{214}Po activity on the filter from other progeny counts, including those of the short-lived radon isotope Radon-220. The methodology and automated algorithm to evaluate the spectra are described in detail by Levin et al. (2002) and Gachkivskyi and Levin (2022). Ambient ^{214}Po activity concentration is then determined from its activity on the filter by considering the filter-detector geometry, the filter efficiency and the mass flow of air through the filter, using the so-called Stockburger algorithm (Stockburger, 1960; Stockburger and Sittkus, 1966). The HRM detection limit of current generation of the monitors is 0.07 Bq m^{-3} (Grossi et al., 2020), with the detection limit being defined as the ambient radon concentration resulting in counting error of 30%. Subsequently, a correction of progeny

loss in the intake tubing (Decabon, 8 mm inner diameter), which can be up to 158 m long (Tab. 1), is then applied following Levin et al. (2017). The length-dependent loss of progeny is approximated by an exponential function

$$R(L) = \exp^{-\frac{L}{L_0}} \tag{1}$$

with L being the length of the tubing and L_0 a constant that was experimentally determined in the laboratory. For a given length of tubing, progeny loss was further observed to be dependent on ambient activity concentration. This could be approximated with a saturation curve as follows:

$$\frac{c_{measured}}{c_{ambient}} = R(L) - A \cdot \exp^{-\frac{c_{measured}}{c_0}} \tag{2}$$

where the experimentally determined empirical parameters A and c_0 are constants, and $R(L)$ is calculated from Eq. 1 for line length L. The constants in Eqs. 1 and 2 have been reported by Levin et al. (2017) to $L_0 = 415$ m, $A = 0.41$ and $c_0 = 0.92$ Bq m^{-3}. The line loss correction was applied to all stations with air intake lines longer than 15 meters, which represents the shortest tested line length for aerosol loss (Levin et al., 2017). No aerosol loss due to the tubing is assumed for lines shorter than 15 meters.

2.3 Calibration and ^{214}Po/^{222}Rn disequilibrium

In a theoretical evaluation, Jacobi and Andre (1963) estimated the height-dependence of the disequilibrium between ^{214}Po and ^{222}Rn. This disequilibrium depends on atmospheric stability and decreases with height, approaching equilibrium at levels of about 100 m a.g.l. In an international comparison experiment of the HRM measuring ^{214}Po with direct ^{222}Rn measurement using an 1500L ANSTO monitor, Schmithüsen et al. (2017) showed that usually equilibrium between ^{222}Rn and ^{214}Po measurements in ambient air is reached at intake heights exceeding 60 m above ground level. However, they found a calibration difference between the two systems of about 10%. A similar result with a slightly smaller difference between monitors was obtained in a comparison campaign conducted in 2017 at the ICOS station Saclay, France, where parallel measurements at the 100 m intake height were conducted (Grossi et al., 2020). At the time of the comparison campaigns, there was no traceable method of calibrating the ANSTO monitor's absolute measurements, as is now the case since the 19ENV01 traceRadon Project (Röttger et al., 2021), which could be accomplished with the Calibration Transfer Standard Devices (Chambers et al., 2022; Röttger et al., 2025). The absence of this calibration could lead to the 4-8% uncertainties in the absolute values (Chambers et al., 2022; Kikaj et al., 2024). This may be a contributing factor to the discrepancies in the two measurement systems. However, the relative concentration changes measured with 1500L ANSTO have been shown to be reliable (Chambers et al., 2022). For this reason, we did not apply any scaling factors to our HRM measurements e.g. to adjust them to the ANSTO scale. Instead, we run each HRM in parallel to our routine monitor in Heidelberg for a few weeks and determine an internal calibration factor that is applied to have comparable measurements within the HRM network. We also did not correct for disequilibrium any of the HRM data from ICOS tower stations with intake heights > 90 m a.g.l., assuming that the atmospheric ^{222}Rn activity

concentration is equal to that of the measured ^{214}Po activity concentration. For the Schauinsland data, we applied a factor of 1/0.8 to the ^{214}Po measurements to estimate ambient ^{222}Rn activity concentrations. This factor corresponds to that reported by Schmithüsen et al. (2017, Table 2).

For the Saclay 2017 comparison campaign, Grossi et al. (2020) showed that the ratio of HRM-measured ^{214}Po and ^{222}Rn measured with the ARMON monitor from Universitat Politècnica de Catalunya (UPC) decreased at relative humidity (RH) values close to 100%. We have re-evaluated the data from this campaign, also correcting the ^{222}Rn measurements from the ANSTO detector for standard temperature and pressure (STP, T = 293.15 K, P = 1000 hPa), to make them comparable with the HRM measurements. These re-evaluated HRM and ANSTO data are displayed in Fig. 2, panel (a) together with the RH measured during that period. The relation between HRM ^{214}Po and ANSTO ^{222}Rn data is displayed in the panel (c). Here we selected the HRM data by distinguishing all hourly values by using co-measured RH data. The pink dots in the panel (c) with RH > 98% clearly deviate from the regression line, with the values from the HRM being lower than the data from ANSTO. This would be consistent with the ^{214}Po aerosols being scavenged during the high RH events. The panel (b) shows the Pearson correlation coefficient between the two data sets dependent on the data selection by RH threshold. This means, that data measured at a lower RH than the threshold is included in the fit calculation. We use the correlation coefficient as the relevant parameter to be investigated because, as discussed in the previous paragraph, there may be other reasons for discrepancies in absolute concentrations between the two measurement systems, such as uncertainties in calibration or instrumental issues that cause systematic biases. A correlation provides a useful tool for examining the relative differences between datasets. A small decrease of the correlation coefficient is observed from 90% to 99% RH, followed by a steep decrease towards 100% RH. Therefore, for this comparison campaign, a relative humidity threshold of 98% would be set to determine a potential "calibration factor" between the two instruments accounting for uncertainty of RH data and ensure the compatibility of the data. Excluding data measured at RH > 98%, we obtain an excellent agreement of almost 1:1 (0.97 ± 0.01) with no significant offset between the HRM and the ANSTO measurements.

2.4 Humidity threshold for the German ^{214}Po/^{222}Rn network

No direct ^{222}Rn observations are available to determine a relative humidity threshold for the German stations with HRM progeny measurements, as was done for the Saclay 2017 campaign (Section 2.3). Therefore, we used a threshold based on the comparison with atmospheric transport model calculations of ^{222}Rn. We used the Stochastic Time-Inverted Lagrangian Transport model STILT (Lin et al., 2003) that was implemented at the ICOS Carbon Portal (https://www.icos-cp.eu/about-stilt) to calculate footprints and atmospheric ^{222}Rn activity concentrations for all ICOS stations. The radon flux estimates for Europe of Karstens and Levin (2023), providing daily mean ^{222}Rn fluxes for the years 2017-2023, were used to calculate hourly ^{222}Rn activity concentrations. We then calculated month-wise correlation coefficients between observed ^{214}Po and modelled ^{222}Rn activity concentrations by successively adding data at increasing observed RH (Kohler et al., 2018; Kubistin et al., 2024a, b, c, d, e, f, g; Schmidt et al., 2024; UBA, 2024; DWD, 2025), similar to the method used for the Saclay 2017 comparison campaign data (Fig. 2 panels (b) and (d)). For this, meteorological data was aggregated to half-hourly values if the measurement frequency was higher than that of ^{222}Rn or interpolated from hourly values. Note that this comparison between

measured ^{214}Po and simulated ^{222}Rn activity concentrations was conducted only to diagnose thresholds for potential ^{214}Po loss at the individual stations. Quantitative evaluations, e.g. of the absolute agreement between model simulations and observations were not target of this comparison, as we are aware that the ^{222}Rn flux map as well as transport in the STILT model have significant uncertainties. We also do not expect good correlations and as smooth curves as were obtained from the comparison of the two measured records at Saclay (Fig. 2, panel (b)). Nevertheless, we assume that a significant and abrupt decrease of correlation coefficient at high RH should also become visible as a consequence of loss of ^{214}Po. This could then be used to pinpoint a threshold of maximum RH at which the radioactive equilibrium of ^{222}Rn and its progeny ^{214}Po is still valid.

Figure 3 shows typical examples of correlation coefficients between modelled ^{222}Rn and measured ^{214}Po (panels (a) and (e)) together with RH distributions at three out of eight stations in the German ICOS network for those hourly situations where ^{214}Po measurements are available. Note that for the mountain stations Schauinsland (SSL, panels (d) and (h)), Torfhaus and Hohenpeißenberg (resp. TOH and HPB, Figs. A1-A12 in Supplementary Material), we did not use STILT results for the actual tower heights (see Tab. 1), but for higher elevations of 300 m (TOH, HPB) and 230 m (SSL), as for these virtual heights model results show better agreement with the observations (Geels et al., 2007; Oney et al., 2015; Kountouris et al., 2018). Panels (b) – (d) in figure 3 show the data from April 2024, a month with a relatively high frequency of RH > 95% at the mountain station of SSL and very few RH values above 90% at the tower stations in flat terrain. The majority of the RH measurements in this month are centered around 60% RH or even lower. All stations show a correlation between measured and modelled data higher than 0.6 if enough data is provided. This could be explained by the fact that for the relatively dry conditions the ^{214}Po concentrations represent the ^{222}Rn values quite well. But it can also be clearly seen that at SSL the correlation coefficient steeply decreases from about 0.65 to about 0.51 if values with RH > 98% are included in the calculation and if the number of these high RH situations becomes significant. The KIT and LIN stations remain largely unchanged in this regard.

In the panels (f) – (h) of figure 3 the corresponding data from November 2022 are shown. In this month RH close to saturation is observed at all stations. However, it is only at very high RH >98% that the correlation coefficient decreases also at the tower stations in flat terrain. Overall, there is a tendency towards higher correlation coefficients between model and observations at the stations located in flat terrain (GAT, STE, KIT, JUE and LIN) compared to the mountain sites (TOH, SSL, HPB). This is because trace gas concentrations at mountain stations, due to their complex topography, are generally less well represented in the model than those in flat terrain. A similar behaviour is observed for the other stations of the German ICOS network and other months of 2022, where we have good overlap of measurements and STILT model results (Figs. A1-A12 in Supplementary Material). In some rare cases, where most data were measured at RH > 98%, a sharp increase in correlation can be observed for high RH values for some stations (e.g. December 2022, Fig. A12). Based on these findings, we suggest to only use ^{214}Po data for the calculation of ^{222}Rn activity concentrations measured at ambient RH < 98%. Secular equilibrium between ^{214}Po and ^{222}Rn can only be assumed for measurements made at RH lower than this threshold. It should be noted that the collection of data published together with this manuscript (Deutscher Wetterdienst et al., 2024a, b, c, d, e, f, g, h) contain all valid ^{214}Po measurements, and we provide a value for ^{222}Rn only for conditions, where full equilibrium between ^{214}Po and ^{222}Rn based on the measured RH can be assumed.

3 Results

Daily mean ^{214}Po data from all stations are shown in the left panel of Fig. 4, while the data remaining after relative humidity flagging (where available) according to the procedure described in Sec. 2.4 are shown in the right panel of Fig. 4. Only mean values for days where more than 70% of the hourly data are available or remained after flagging are displayed. Where no RH data is available, the ^{214}Po data has been flagged. At some of the sites there are large gaps in the ^{214}Po data, which are due to initial handling and logistical problems or occasional HRM failures. After flagging, data gaps become more frequent, especially during winter at high RH and at mountain stations like SSL and TOH, where the high RH events are more prevalent in general. On average, we observe the highest ^{214}Po (and ^{222}Rn) activity concentrations at KIT located in the upper Rhine valley. Even the mountain stations, which usually have longer air mass transport away from the ^{222}Rn source and hence lower concentrations, SSL and HPB show elevated concentrations compared to the rest of the network, with both of them and KIT located in the south of Germany. The lowest activity concentrations are found at GAT, STE and TOH with JUE showing slightly higher ^{214}Po activities. All these stations are situated in the northern half of Germany. This south-north gradient of the ^{222}Rn concentration is consistent with the radon flux estimates for Europe derived from uranium soil content, soil properties and moisture content by Karstens and Levin (2023). Another factor contributing to this gradient may be the increased influence of radon-depleted marine air masses on northern stations. These stations are situated closer to the basins of the North Sea and the Baltic Sea with negligible radon flux from the surface. On the other hand, air masses reaching the southern stations potentially have more time for radon emanating from the soil to mix into them, leading to higher observed concentrations. The only exception to this longitudinal scheme is the LIN station that, however, has a region of elevated radon soil emission values to the south of the station.

At all stations we find a clear seasonal cycle with highest values in summer and autumn and lowest activity concentrations in winter and spring (Fig. 5 shows KIT, SSL and LIN, and A13 in Supplementary Material depicts all stations). This seasonality is mainly caused by the seasonality of the radon exhalation rate from soils, which, on the seasonal time scale, is mainly driven by soil moisture (Karstens et al., 2015). The high ^{222}Rn values in summer and autumn are also due to stable atmospheric conditions in these seasons during nights (cf. Fig. 6) as well as to more frequent high-pressure systems bringing continental air masses to Germany.

The mean diurnal cycles of ^{222}Rn from January to December 2022 are displayed in Fig. 6. Only in summer and early autumn (i.e. from April to September) we observe on average significant diurnal variations at the tower stations in flat terrain with maximum values early in the morning after sunrise, i.e. shortly before the atmosphere becomes well-mixed and ^{222}Rn that was accumulated close to the ground is mixed into higher levels of the troposphere. At HPB the morning maximum occurs with a few hours delay, as ground level radon is not only transported through vertical convection but also by upslope winds from the surrounding valleys to the sampling site. A similar diurnal variation is observed at SSL in some of the summer and autumn months. This behaviour of ^{222}Rn had already been observed earlier by Levin (1987). During late autumn, winter and early spring, systematic diurnal variations are missing at all sites as the variations of the ^{222}Rn activity concentration are much more dominated by synoptic variations. This could be explained by smaller differences in the daily and nightly mixing height

distributions during late autumn and winter months (Emeis and Turk, 2004), which would greatly diminish radon diurnal amplitude.

4 Discussion and Conclusions

Currently, there are eight ICOS stations within Germany measuring atmospheric ^{214}Po/^{222}Rn activity concentrations; these are fairly even distributed over the country with 5 tall towers in flat terrain and 3 stations on mountain tops (two of which are sampling air from more than 90 m above ground level). Observations are conducted with the static filter Heidelberg Radon Monitor, measuring atmospheric ^{222}Rn progeny. At all tower stations sampling air from intake heights more than 90 m above ground level, progeny can be assumed in equilibrium with atmospheric ^{222}Rn. Only at very high relative humidity > 98% this is not necessarily the case, which we were able to demonstrate by comparison with simulated ^{222}Rn activity concentrations. We, therefore, recommend excluding the data measured with HRM during the RH conditions of 98% and above at all sites in any applications where ^{222}Rn values are of interest (and not of its progenies) for example as a tracer for boundary layer transport e.g. for atmospheric transport model validation or for the application of the Radon-Tracer-Method (RTM Levin et al., 2021). In this latter application, the missing data at high RH will probably not cause additional uncertainty in RTM-based flux estimates, because these very humid atmospheric situations with marine air reaching the stations normally show little correlation between GHGs concentrations and ^{222}Rn, and such situations would have been discarded. In the case of atmospheric transport model validation, however, it is essential to use appropriately flagged radon data, where the equilibrium between radon and its progenies can be ensured, even if this results in data gaps. The scavenging of aerosols in small droplets, followed by wet deposition and rain out, can cause a significant reduction in radon progenies, which leads to discrepancies with radon signal. These findings further highlight the limitations of the HRMs and the need for direct ^{222}Rn measurements at the high altitude sites where clouds frequently coincide with the intake heights. The amount of flagged data ranges from 3% to 55% in the wetter winter months (December – February, average 24%), with highest flagged percentage in TOH (51%) and SSL (55%), and lowest in KIT (9%) and JUE (3%). During the dryer summer months (June – August), percentage of flagged observations is significantly lower (average 7%), with the same stations for highest and lowest amounts (high: TOH – 13%, SSL – 16%, low: KIT – 1%, JUE – 1%).

In view of the rather small percentage of the data where the ^{214}Po data measured with the HRM were most probably not in secular equilibrium with ^{222}Rn (with exception of SSL and TOH stations during winter months), and since the absolute agreement between the HRM and other instruments measuring ^{222}Rn directly was in the order of $\pm$10% during intercomparison campaigns, we conclude that our method is suitable for sampling heights above 80-90 m a.g.l for the stations in the flat terrain. The situation may be different for lower intake heights, where we cannot generally assume radioactive equilibrium between ^{222}Rn and its progenies. For example, in the case of our station in Heidelberg, where air is collected from the roof of the building at 30 m a.g.l., we have to apply a mean correction for disequilibrium, multiplying the ^{214}Po activity concentration with a corresponding factor that was based on comparison measurements with an ANSTO detector (i.e. 1.11 Schmithüsen et al., 2017; Levin et al., 2021). A correction for disequilibrium also must be applied to the Schauinsland ^{214}Po data based on

comparison with direct ^{222}Rn measurements (Xia et al., 2010). As the disequilibrium between ^{214}Po and ^{222}Rn depends on atmospheric stability (Jacobi and Andre, 1963; Cuntz, 1997), applying just one mean factor adds uncertainty to the ^{222}Rn data. Measuring ^{222}Rn gradients below 80-90 m a.g.l. is, therefore, not recommended with the HRM, unless a careful comparison with an instrument measuring ^{222}Rn directly has been conducted for each height level, in order to apply a disequilibrium correction based on direct observations. Furthermore, for high-altitude stations (e.g. TOH or SSL) with a high prevalence of RH values greater than 98%, it is essential to closely examine the typical meteorological conditions prior to HRM deployment or to consider the utilisation of other radon instruments that are not prone to aerosol scavenging effects.

5 Data availability

The ^{222}Rn observations are available at the ICOS Carbon Portal (https://doi.org/10.18160/Q2M8-B1HJ, Deutscher Wetterdienst et al., 2024a, b, c, d, e, f, g, h).

Appendix A

A1

Author contributions. MG evaluated all raw data, conducted the relative humidity selection and prepared the figures. UK made the STILT model runs. BF, ML, DK, JMW provided the observational data. IL together with UK and MG designed the study and prepared the manuscript. All authors discussed and reviewed the manuscript.

Competing interests. The authors declare that they have no conflict of interest.

Acknowledgements. We wish to thank the German Meteorological Service station technicians for their support in radon measurement and maintenance. The HRM instrumentation was partly funded by the Federal Ministry of Education and Research and the Federal Ministry for Digital and Transport. This study was supported by the ICOS Central Radiocarbon Laboratory, which is funded by the German Federal Ministry for Digital and Transport. Ute Karstens received funding from the project 19ENV01 traceRadon, part of the EMPIR program that is co-financed by the Participating States and from the European Union's Horizon 2020 research and innovation program. We would like to express our sincere gratitude to Samuel Hammer for his valuable time and insightful comments on this manuscript.

References

Biraud, S.: Vers la régionalisation des puits et sources des composes à effet de serre: analyse de la variabilité synoptique à l'observatoire de Mace Head, Irlande, Ph.D. thesis, Paris 7, 2000.

Chambers, S., Williams, A., Zahorowski, W., Griffiths, A., and Crawford, J.: Separating remote fetch and local mixing influences on vertical radon measurements in the lower atmosphere, Tellus B: Chemical and Physical Meteorology, 63, 843–859, 2011.

Chambers, S. D., Griffiths, A. D., Williams, A. G., Sisoutham, O., Morosh, V., Röttger, S., Mertes, F., and Röttger, A.: Portable two-filter dual-flow-loop 222 Rn detector: Stand-alone monitor and calibration transfer device, Advances in Geosciences, 57, 63–80, 2022.

Cuntz, M.: The Heidelberg 222Rn monitor: Calibration, optimisation, application, Ph.D. thesis, Diploma Thesis, Institut für Umweltphysik, Heidelberg University, Germany, 1997.

Deutscher Wetterdienst, M. O. H., Kubistin, D., Fischer, B., Lindauer, M., Kneuer, T., Müller-Williams, J., and Plaß-Dülmer, C.: Atmospheric measurements results archive, Gartow (132.0 m), 2016-03-02–2024-09-30, https://hdl.handle.net/11676/9YtHV9lv_z-5NpWsaXIyghMD, 2024a.

Deutscher Wetterdienst, M. O. H., Kubistin, D., Fischer, B., Lindauer, M., Kneuer, T., Müller-Williams, J., and Plaß-Dülmer, C.: Atmospheric measurements results archive, Hohenpeissenberg (93.0 m), 2014-10-01–2024-09-30, https://hdl.handle.net/11676/ZVaCsTVBdeJr_jsnB120Nwc1, 2024b.

Deutscher Wetterdienst, M. O. H., Kubistin, D., Fischer, B., Lindauer, M., Kneuer, T., Müller-Williams, J., and Plaß-Dülmer, C.: Atmospheric measurements results archive, Jülich (120.0 m), 2021-07-22–2024-09-30, https://hdl.handle.net/11676/dhOeUioVdRc9dbpYewXMRwke, 2024c.

Deutscher Wetterdienst, M. O. H., Kubistin, D., Fischer, B., Lindauer, M., Kneuer, T., Müller-Williams, J., and Plaß-Dülmer, C.: Atmospheric measurements results archive, Karlsruhe (100.0 m), 2017-06-30–2024-09-30, https://hdl.handle.net/11676/pd9FRefuEbZLAXzP9M4WvU3B, 2024d.

Deutscher Wetterdienst, M. O. H., Kubistin, D., Fischer, B., Lindauer, M., Kneuer, T., Müller-Williams, J., and Plaß-Dülmer, C.: Atmospheric measurements results archive, Lindenberg (98.0 m), 2015-03-09–2024-09-30, https://hdl.handle.net/11676/dRi26ETEDj_T4RN--DiOjdhC, 2024e.

Deutscher Wetterdienst, M. O. H., Kubistin, D., Fischer, B., Lindauer, M., Kneuer, T., Müller-Williams, J., and Plaß-Dülmer, C.: Atmospheric measurements results archive, Steinkimmen (127.0 m), 2020-03-03–2024-09-30, https://hdl.handle.net/11676/9wL0RYQKs1UY7CIoRnHL-Pmz, 2024f.

Deutscher Wetterdienst, M. O. H., Kubistin, D., Fischer, B., Lindauer, M., Kneuer, T., Müller-Williams, J., and Plaß-Dülmer, C.: Atmospheric measurements results archive, Torfhaus (110.0 m), 2018-06-21–2024-09-30, https://hdl.handle.net/11676/mGQi5M3r9fWyczFjbaK88k1z, 2024g.

Deutscher Wetterdienst, M. O. H., Lindauer, M., Kubistin, D., Fischer, B., Schmidt, M., Schumacher, M., Kneuer, T., Müller-Williams, J., and Plaß-Dülmer, C.: Atmospheric measurements results archive, Schauinsland (12.0 m), 2014-02-21–2024-09-30, https://hdl.handle.net/11676/j_6dw4_39JB-N6EFh4eXqZsv, 2024h.

Dörr, H., Kromer, B., Levin, I., Münnich, K., and Volpp, H.-J.: CO2 and radon 222 as tracers for atmospheric transport, Journal of Geophysical Research: Oceans, 88, 1309–1313, 1983.

DWD: Deutscher Wetterdienst, Unpublished meteorogical data for LIN (98 m) and HPB (131 m), available upon request, publication in preparation, contact: Dagmar Kubistin (dagmar.kubistin@dwd.de), Matthias Lindauer (matthias.lindauer@dwd.de), Jennifer Müller-Williams (jennifer.mueller-williams@dwd.de), 2025.

Emeis, S. and Turk, M.: Frequency distributions of the mixing height over an urban area from SODAR data, Meteorologische Zeitschrift, 13, 361–368, 2004.

Gachkivskyi, M. and Levin, I.: User Manual of the Heidelberg Radon Monitor, https://doi.org/10.18160/BWHB-KFAJ, 2022.

Geels, C., Gloor, M., Ciais, P., Bousquet, P., Peylin, P., Vermeulen, A., Dargaville, R., Aalto, T., Brandt, J., Christensen, J., et al.: Comparing atmospheric transport models for future regional inversions over Europe–Part 1: mapping the atmospheric CO 2 signals, Atmospheric Chemistry and Physics, 7, 3461–3479, 2007.

Grossi, C., Àgueda, A., Vogel, F., Vargas, A., Zimnoch, M., Wach, P., Martín, J., López-Coto, I., Bolívar, J., Morguí, J. A., et al.: Analysis of ground-based 222Rn measurements over Spain: Filling the gap in southwestern Europe, Journal of Geophysical Research: Atmospheres, 121, 11–021, 2016.

Grossi, C., Vogel, F. R., Curcoll, R., Àgueda, A., Vargas, A., Rodó, X., and Morguí, J.-A.: Study of the daily and seasonal atmospheric CH 4 mixing ratio variability in a rural Spanish region using 222 Rn tracer, Atmospheric chemistry and physics, 18, 5847–5860, 2018.

Grossi, C., Chambers, S. D., Llido, O., Vogel, F. R., Kazan, V., Capuana, A., Werczynski, S., Curcoll, R., Delmotte, M., Vargas, A., et al.: Intercomparison study of atmospheric 222 Rn and 222 Rn progeny monitors, Atmospheric Measurement Techniques, 13, 2241–2255, 2020.

ICOS RI: ICOS Atmosphere Station Specifications V2.0 (editor: O. Laurent), https://doi.org/10.18160/GK28-2188, 2020.

Jacob, D. J. and Prather, M. J.: Radon-222 as a test of convective transport in a general circulation model, Tellus B, 42, 118–134, 1990.

Jacob, D. J., Prather, M. J., Rasch, P. J., Shia, R.-L., Balkanski, Y. J., Beagley, S. R., Bergmann, D. J., Blackshear, W., Brown, M., Chiba, M., et al.: Evaluation and intercomparison of global atmospheric transport models using 222Rn and other short-lived tracers, Journal of Geophysical Research: Atmospheres, 102, 5953–5970, 1997.

Jacobi, W. and Andre, K.: The vertical distribution of radon 222, radon 220 and their decay products in the atmosphere, Journal of Geophysical Research, 68, 3799–3814, 1963.

Karstens, U. and Levin, I.: traceRadon daily radon flux map for Europe 2022 (based on GLDAS-Noah v2.1 soil moisture), https://hdl.handle.net/11676/SG_LHGMUsZVv9NxkIrRw9eRv, daily radon flux map for Europe 2022 based on soil uranium content (EANR, 2019, https://data.europa.eu/doi/10.2760/520053), soil properties (ESDB, Hiederer, 2013, https://doi.org/10.2788/94128), and GLDAS-Noah v2.1 soil moisture reanalysis (Beaudoing and Rodell, 2020, https://doi.org/10.5067/E7TYRXPJKWOQ). The radon flux model is described in Karstens et al., 2015, https://doi.org/10.5194/acp-15-12845-2015., 2023.

Karstens, U., Schwingshackl, C., Schmithüsen, D., and Levin, I.: A process-based 222 radon flux map for Europe and its comparison to long-term observations, Atmospheric Chemistry and Physics, 15, 12 845–12 865, 2015.

Kikaj, D., Chung, E., Griffiths, A. D., Chambers, S. D., Foster, G., Wenger, A., Pickers, P., Rennick, C., O'doherty, S., Pitt, J., et al.: Direct high-precision radon quantification for interpreting high frequency greenhouse gas measurements, Atmospheric Measurement Techniques Discussions, 2024, 1–37, 2024.

Kohler, M., Metzger, J., and Kalthoff, N.: Trends in temperature and wind speed from 40 years of observations at a 200-m high meteorological tower in Southwest Germany, International Journal of Climatology, 38, 23–34, 2018.

Kountouris, P., Gerbig, C., Rödenbeck, C., Karstens, U., Koch, T. F., and Heimann, M.: Atmospheric CO 2 inversions on the mesoscale using data-driven prior uncertainties: methodology and system evaluation, Atmospheric Chemistry and Physics, 18, 3027–3045, 2018.

Kubistin, D., Plaß-Dülmer, C., Arnold, S., Kneuer, T., Lindauer, M., and Müller-Williams, J.: ICOS ATC Meteo Release, Karlsruhe (100.0 m), 2019-08-01–2024-03-31, https://hdl.handle.net/11676/6F7MBUvIk-jTUs77bMSN7vPz, 2024a.

Kubistin, D., Plaß-Dülmer, C., Arnold, S., Kneuer, T., Lindauer, M., and Müller-Williams, J.: ICOS ATC Meteo Release, Steinkimmen (127.0 m), 2019-07-22–2024-03-31, https://hdl.handle.net/11676/S9-m-RTwRNjSSJ1YUv-uScKs, 2024b.

Kubistin, D., Plaß-Dülmer, C., Arnold, S., Kneuer, T., Lindauer, M., Müller-Williams, J., and Schumacher, M.: ICOS ATC Meteo Release, Gartow (132.0 m), 2016-05-10–2024-03-31, https://hdl.handle.net/11676/dLToI172WS2PKvvwgvV1jWAf, 2024c.

Kubistin, D., Plaß-Dülmer, C., Arnold, S., Kneuer, T., Lindauer, M., Müller-Williams, J., and Schumacher, M.: ICOS ATC Meteo Release, Hohenpeissenberg (93.0 m), 2015-09-18–2024-03-31, https://hdl.handle.net/11676/ZgapN6ANw2V2YFM9pjdsqy4r, 2024d.

Kubistin, D., Plaß-Dülmer, C., Arnold, S., Kneuer, T., Lindauer, M., Müller-Williams, J., and Schumacher, M.: ICOS ATC Meteo Release, Lindenberg (98.0 m), 2017-02-21–2024-03-31, https://hdl.handle.net/11676/ejumpR8yaFWEp6XWrOUW88Hj, 2024e.

Kubistin, D., Plaß-Dülmer, C., Arnold, S., Kneuer, T., Lindauer, M., Müller-Williams, J., and Schumacher, M.: ICOS ATC Meteo Release, Torfhaus (110.0 m), 2018-06-21–2024-03-31, https://hdl.handle.net/11676/qOdruveyxvVFPIriXkBTc3k9, 2024f.

Kubistin, D., Plaß-Dülmer, C., Kneuer, T., Lindauer, M., and Müller-Williams, J.: ICOS ATC Meteo Release, Jülich (120.0 m), 2021-07-23–2024-03-31, https://hdl.handle.net/11676/C7bjmdaMVMOPWmSMKOGXsyE0, 2024g.

Levin, I.: Atmospheric CO2 in continental Europe — an alternative approach to clean air CO2 data, Tellus B, 39, 21–28, 1987.

Levin, I., Glatzel-Mattheier, H., Marik, T., Cuntz, M., Schmidt, M., and Worthy, D. E.: Verification of German methane emission inventories and their recent changes based on atmospheric observations, Journal of Geophysical Research: Atmospheres, 104, 3447–3456, 1999.

Levin, I., Born, M., Cuntz, M., Langendörfer, U., Mantsch, S., Naegler, T., Schmidt, M., Varlagin, A., Verclas, S., and Wagenbach, D.: Observations of atmospheric variability and soil exhalation rate of radon-222 at a Russian forest site. Technical approach and deployment for boundary layer studies, Tellus B: Chemical and Physical Meteorology, 54, 462–475, 2002.

Levin, I., Schmithüsen, D., and Vermeulen, A.: Assessment of 222 radon progeny loss in long tubing based on static filter measurements in the laboratory and in the field, Atmospheric Measurement Techniques, 10, 1313–1321, 2017.

Levin, I., Karstens, U., Hammer, S., DellaColetta, J., Maier, F., and Gachkivskyi, M.: Limitations of the radon tracer method (RTM) to estimate regional greenhouse gas (GHG) emissions–a case study for methane in Heidelberg, Atmospheric Chemistry and Physics, 21, 17 907–17 926, 2021.

Levin, I., Gachkivskyi, M., and Botía, S.: Activity concentration of Radon (222Rn) at the ATTO site (2018 to 2024), https://doi.org/10.17871/ATTO.487.8.2038, 2025.

Lin, J., Gerbig, C., Wofsy, S., Andrews, A., Daube, B., Davis, K., and Grainger, C.: A near-field tool for simulating the upstream influence of atmospheric observations: The Stochastic Time-Inverted Lagrangian Transport (STILT) model, Journal of Geophysical Research: Atmospheres, 108, 2003.

Nazaroff, W. W.: Radon transport from soil to air, Reviews of geophysics, 30, 137–160, 1992.

Oney, B., Henne, S., Gruber, N., Leuenberger, M., Bamberger, I., Eugster, W., and Brunner, D.: The CarboCount CH sites: characterization of a dense greenhouse gas observation network, Atmospheric chemistry and physics, 15, 11 147–11 164, 2015.

Paatero, J., Hatakka, J., and Viisanen, Y.: Concurrent measurements of airborne radon-222, lead-210 and beryllium-7 at the Pallas-Sodankylä GAW station, Northern Finland, Ilmatieteen laitos, 1998.

Polian, G.: Les transports atmosphériques dans l'hémisphère sud et le bilan global du radon-222, Ph.D. thesis, PhD Thesis, University of Paris VI, France, 1986.

Röttger, A., Röttger, S., Grossi, C., Vargas, A., Curcoll, R., Otáhal, P., Hernández-Ceballos, M. Á., Cinelli, G., Chambers, S., Barbosa, S. A., et al.: New metrology for radon at the environmental level, Measurement Science and Technology, 32, 124 008, 2021.

Röttger, S., Röttger, A., Mertes, F., Chambers, S., Griffiths, A., Curcoll, R., and Grossi, C.: Traceable low activity concentration calibration of radon detectors for climate change observation networks, Measurement: Sensors, p. 101708, 2025.

Schery, S. and Huang, S.: An estimate of the global distribution of radon emissions from the ocean, Geophysical Research Letters, 31, 2004.

Schmidt, M., Hoheisel, A., and Meinhardt, F.: ICOS ATC Meteo Release, Schauinsland (1.5 m), 2021-08-02–2024-03-31, https://hdl.handle.net/11676/6OVRGfa0RVGoU6m3aYF3joxJ, 2024.

Schmithüsen, D., Chambers, S., Fischer, B., Gilge, S., Hatakka, J., Kazan, V., Neubert, R., Paatero, J., Ramonet, M., Schlosser, C., et al.: A European-wide 222 radon and 222 radon progeny comparison study, Atmospheric Measurement Techniques, 10, 1299–1312, 2017.

Stockburger, H.: Continuous registration of the radon-, thorium-B and decay product activity of atmospheric air, Ph.D. thesis, PhD Thesis, University of Freiburg, Germany (in German), 1960.

Stockburger, H. and Sittkus, A.: Unmittelbare Messung der natürlichen und künstlichen Radioaktivität der atmosphärischen Luft, Zeitschrift für Naturforschung A, 21, 1128–1132, 1966.

Taguchi, S., Law, R., Rödenbeck, C., Patra, P., Maksyutov, S., Zahorowski, W., Sartorius, H., and Levin, I.: TransCom continuous experiment: comparison of 222 Rn transport at hourly time scales at three stations in Germany, Atmospheric Chemistry and Physics, 11, 10 071–10 084, 2011.

UBA: Umweltbundesamt, Unpublished data meteorogical data, available from Stefan Feigenspan upon request, humidity sensor - "DEUB004", stefan.feigenspan@uba.de, 2024.

Weller, R., Levin, I., Schmithüsen, D., Nachbar, M., Asseng, J., and Wagenbach, D.: On the variability of atmospheric 222 Rn activity concentrations measured at Neumayer, coastal Antarctica, Atmospheric Chemistry and Physics, 14, 3843–3853, 2014.

Whittlestone, S. and Zahorowski, W.: Baseline radon detectors for shipboard use: Development and deployment in the First Aerosol Characterization Experiment (ACE 1), Journal of Geophysical Research: Atmospheres, 103, 16 743–16 751, 1998.

Williams, A. G., Zahorowski, W., Chambers, S., Griffiths, A., Hacker, J. M., Element, A., and Werczynski, S.: The vertical distribution of radon in clear and cloudy daytime terrestrial boundary layers, Journal of the Atmospheric Sciences, 68, 155–174, 2011.

Xia, Y., Sartorius, H., Schlosser, C., Stöhlker, U., Conen, F., and Zahorowski, W.: Comparison of one-and two-filter detectors for atmospheric 222 Rn measurements under various meteorological conditions, Atmospheric Measurement Techniques, 3, 723–731, 2010.

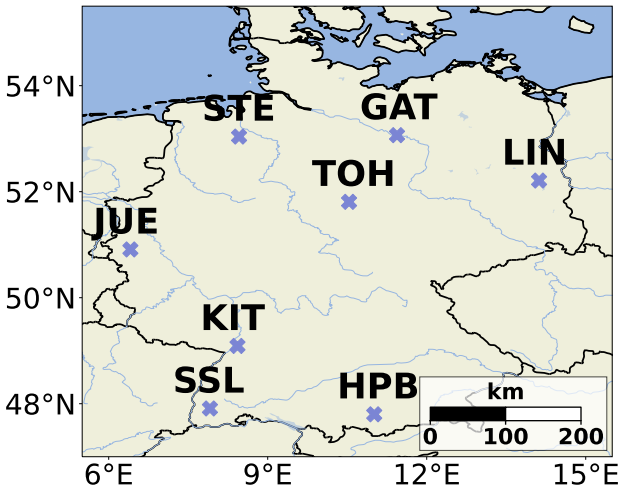

Figure 1. Radon measurements in Germany are conducted with the HRM at eight ICOS atmosphere stations. All stations except for SSL are tall towers operated by DWD (radon intake heights between 93 m and 132 m a.g.l.). SSL has its air intake at 12 m a.g.l. and is operated by the German Environment Agency.

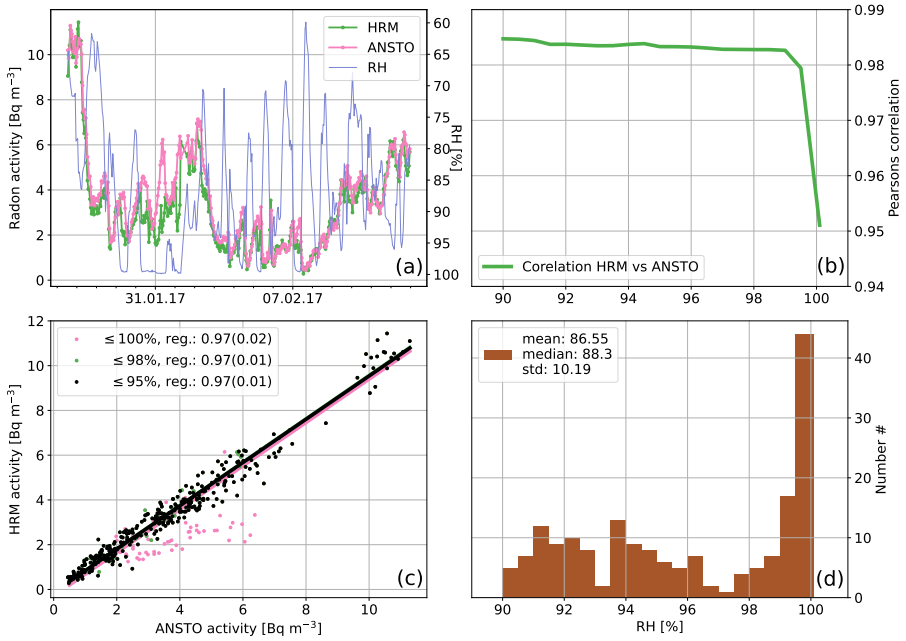

Figure 2. Activity concentration measured with the ANSTO monitor and with the HRM during the 2017 comparison campaign at Saclay tower at the 100m level. The panel (a) shows the original records together with relative humidity (the frequency distribution of RH is shown in the panel (d)). The panel (c) displays the regression lines between the two datasets with some data being excluded depending on the co-measured RH values. The data is obtained at RH less than or equal to 95% and the additions to this set with RH less than or equal to 98% are highlighted in green. Data measured at RH > 98% up to 100% are marked in pink. The data with RH > 98% (in pink) clearly fall off the regression line. The panel (b) shows the development of the Pearson correlation coefficient when successively more data measured at higher RH are included in the correlation calculation.

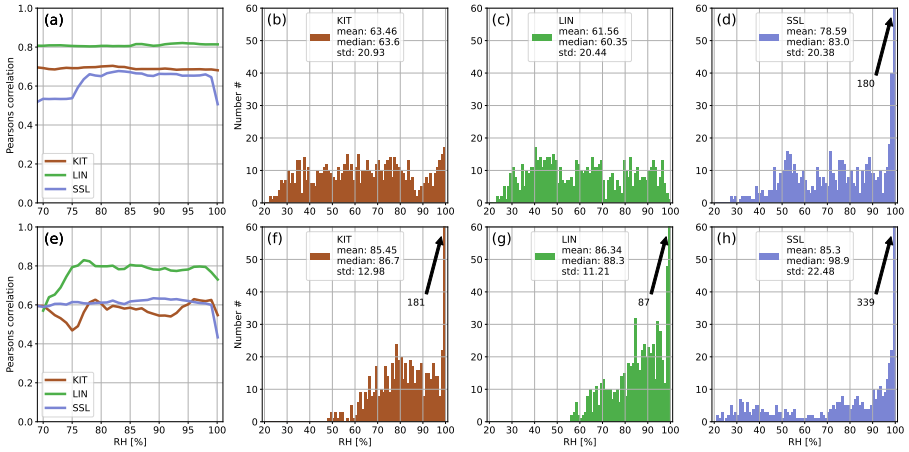

Figure 3. The panels (a) and (e) show the development of the correlation coefficient between ^{214}Po observations and simulated ^{222}Rn data at three German ICOS stations (KIT, LIN, SSL) for April and for November 2022 respectively if data with increasing RH are successively included in the calculation of the correlation. The panels (b) – (d) and (f) – (h) show the RH distributions for April and November respectively at these stations that were included in the calculations.The arrows with numbers indicate values that exceed the y-axis range (usually for high RH). For each station the correlation coefficient was calculated only if the number of filtered data points was higher than 10% of all values for the given month to avoid the stochastic behavior of the curves in the panels (a) and (e) associated with small data sets.

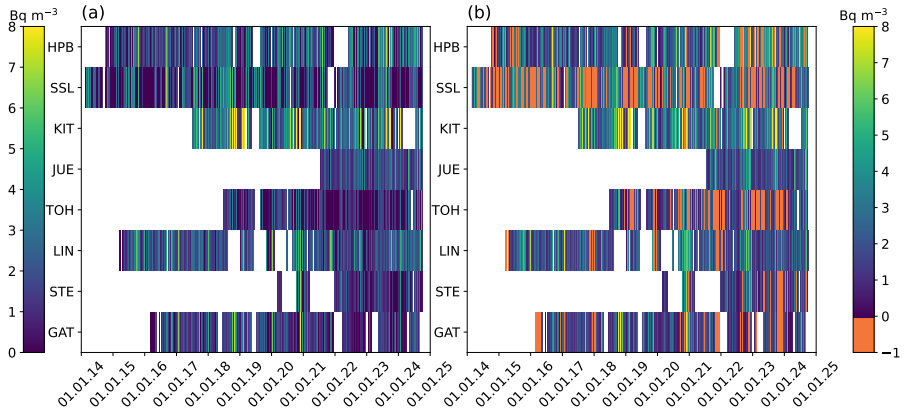

Figure 4. Panel (a) shows daily mean atmospheric ^{214}Po activity concentrations in Bq m^{-3} at German ICOS stations. The daily values are plotted only if more than 70% of the hourly data was available. The panel (b) shows all valid data where measurements were conducted at RH below the respective thresholds and thus represent the best estimates of the RH-selected ^{222}Rn data. The periods where less than 70% of the hourly data remained after flagging are shown in orange (with values of -1).

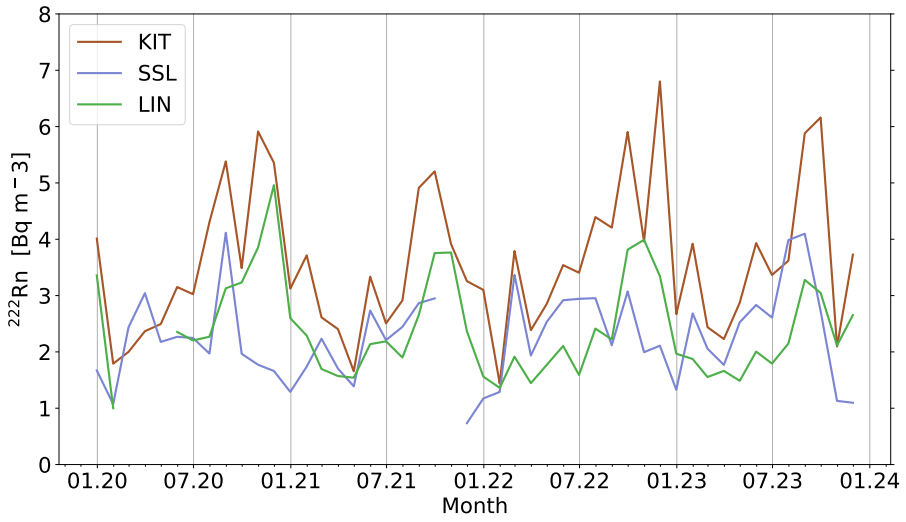

Figure 5. Seasonal cycle of ^{222}Rn monthly means at KIT, SSL and LIN in the time period of 2020-2023. Note that monthly values are only shown if more than 70% of the daily mean values were available for the respective month.

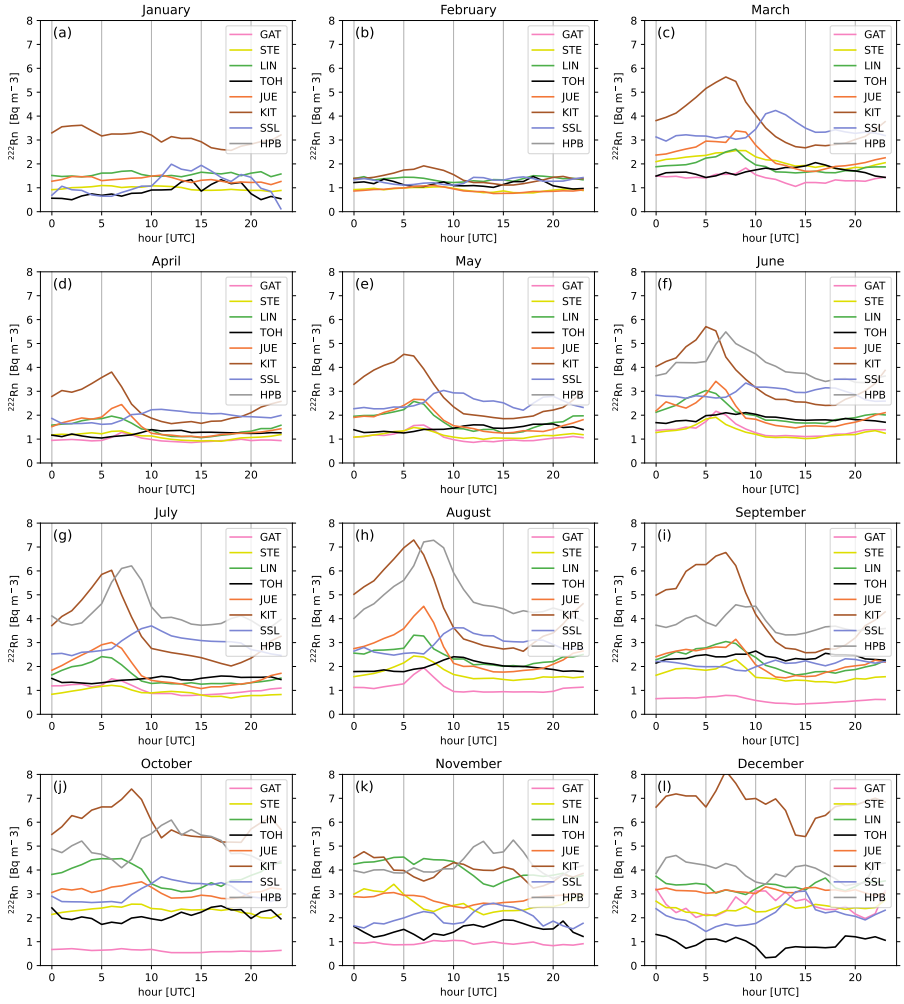

Figure 6. Mean diurnal cycles of ^{214}Po-based ^{222}Rn for all months in 2022 where data is available.

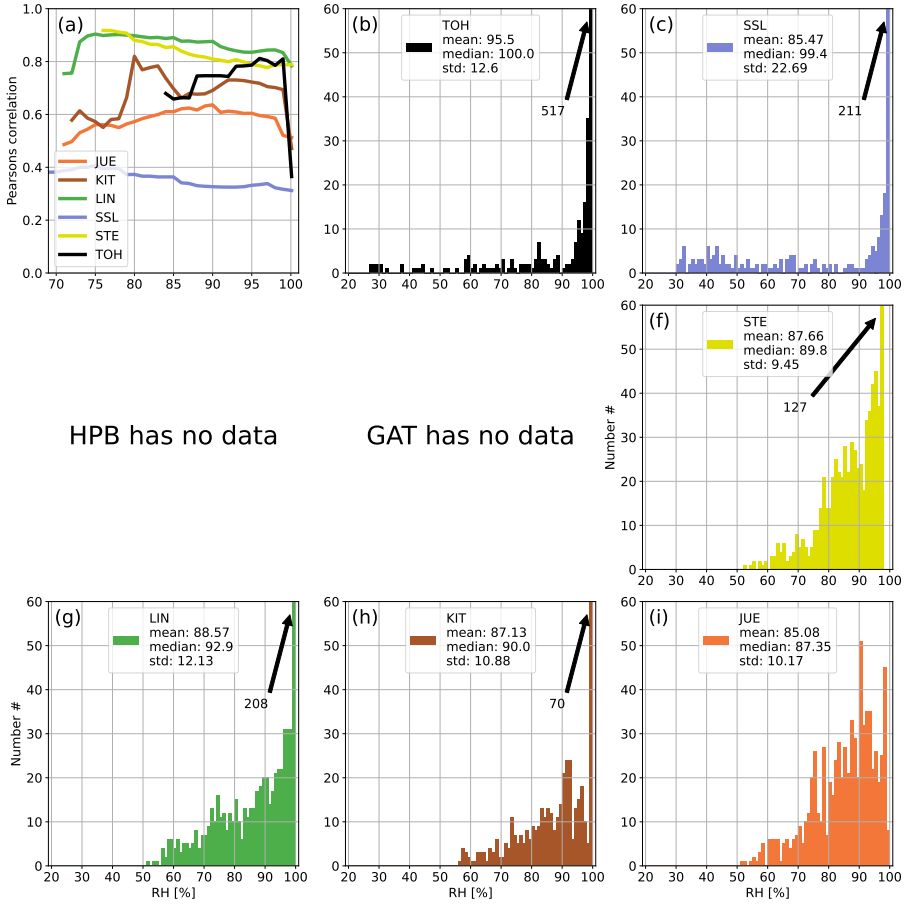

Figure A1. The panel (a) shows the development of the correlation coefficient between ^{214}Po observations and simulated ^{222}Rn data at all German ICOS stations if data with increasing RH are successively included in the calculation of the correlation. The panels (b) – (i) show the distributions of hourly RH values at the stations of the network. The arrows with numbers indicate values that exceed the y-axis range (usually for high RH). For each station the correlation coefficient was calculated only if the number of filtered data points was higher than 10% of all values for the given month to avoid the stochastic behaviour of the curves in the first subplot associated with small data sets. January 2022.

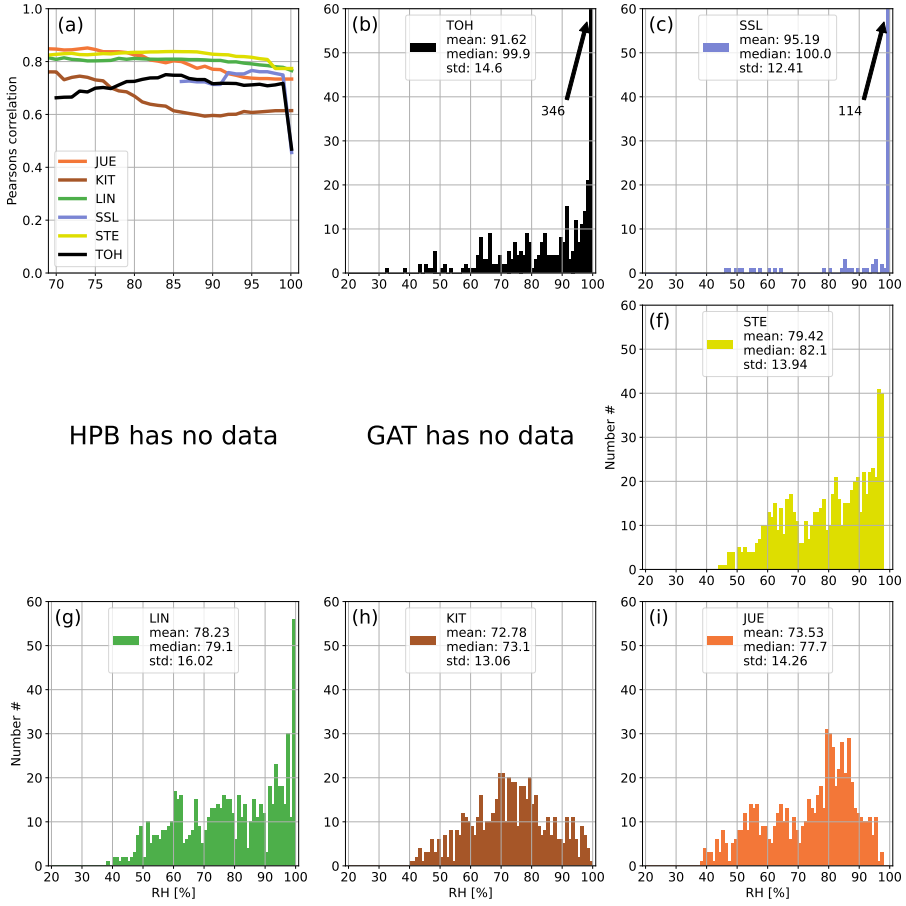

Figure A2. The panel (a) shows the development of the correlation coefficient between ^{214}Po observations and simulated ^{222}Rn data at all German ICOS stations if data with increasing RH are successively included in the calculation of the correlation. The panels (b) – (i) show the distributions of hourly RH values at the stations of the network. The arrows with numbers indicate values that exceed the y-axis range (usually for high RH). For each station the correlation coefficient was calculated only if the number of filtered data points was higher than 10% of all values for the given month to avoid the stochastic behaviour of the curves in the first subplot associated with small data sets. February 2022.

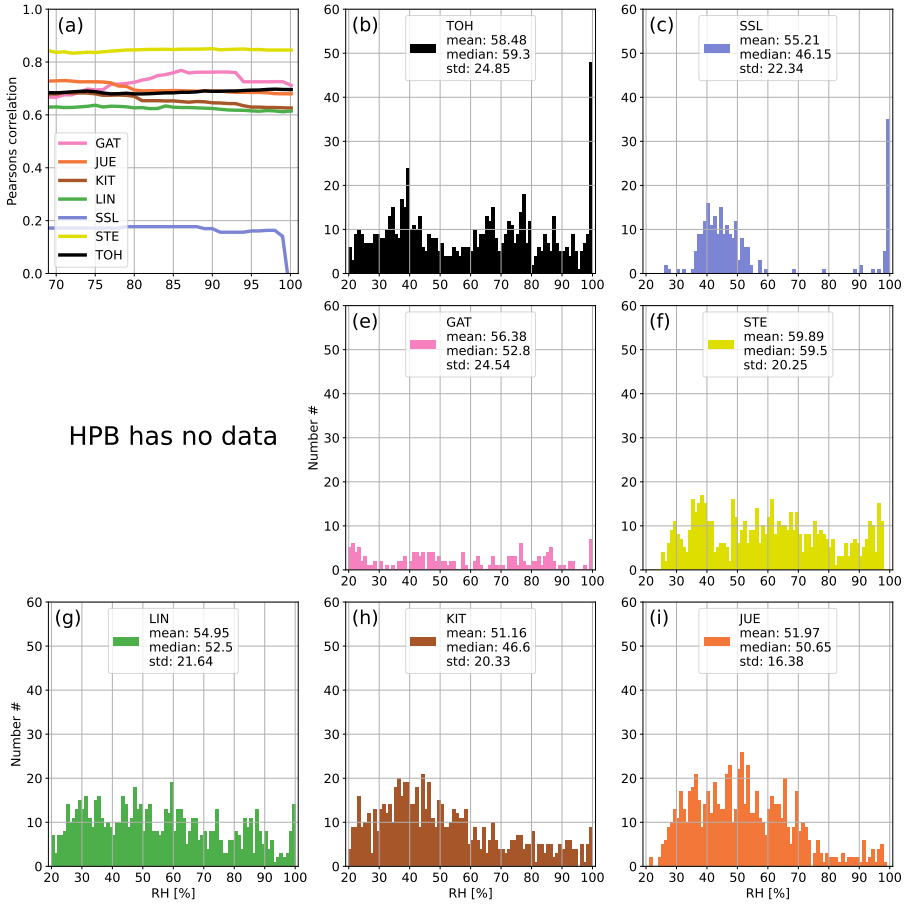

Figure A3. The panel (a) shows the development of the correlation coefficient between ^{214}Po observations and simulated ^{222}Rn data at all German ICOS stations if data with increasing RH are successively included in the calculation of the correlation. The panels (b) – (i) show the distributions of hourly RH values at the stations of the network. The arrows with numbers indicate values that exceed the y-axis range (usually for high RH). For each station the correlation coefficient was calculated only if the number of filtered data points was higher than 10% of all values for the given month to avoid the stochastic behaviour of the curves in the first subplot associated with small data sets. March 2022.

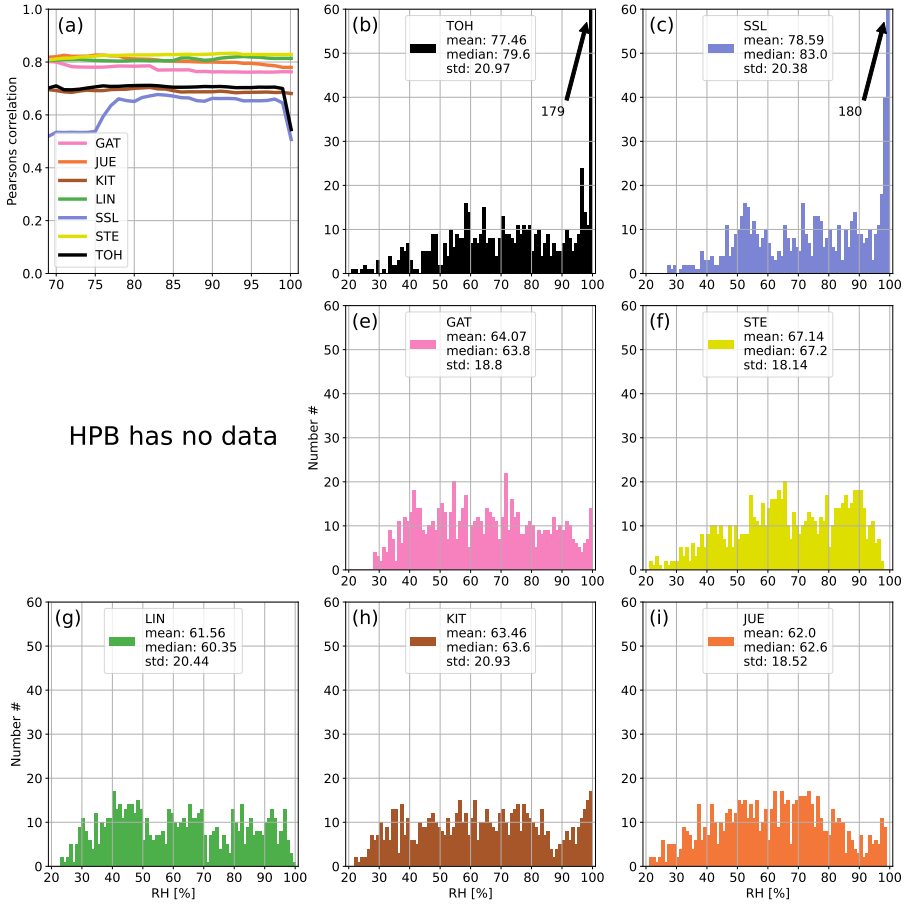

Figure A4. The panel (a) shows the development of the correlation coefficient between ^{214}Po observations and simulated ^{222}Rn data at all German ICOS stations if data with increasing RH are successively included in the calculation of the correlation. The panels (b) – (i) show the distributions of hourly RH values at the stations of the network. The arrows with numbers indicate values that exceed the y-axis range (usually for high RH). For each station the correlation coefficient was calculated only if the number of filtered data points was higher than 10% of all values for the given month to avoid the stochastic behaviour of the curves in the first subplot associated with small data sets. April 2022.

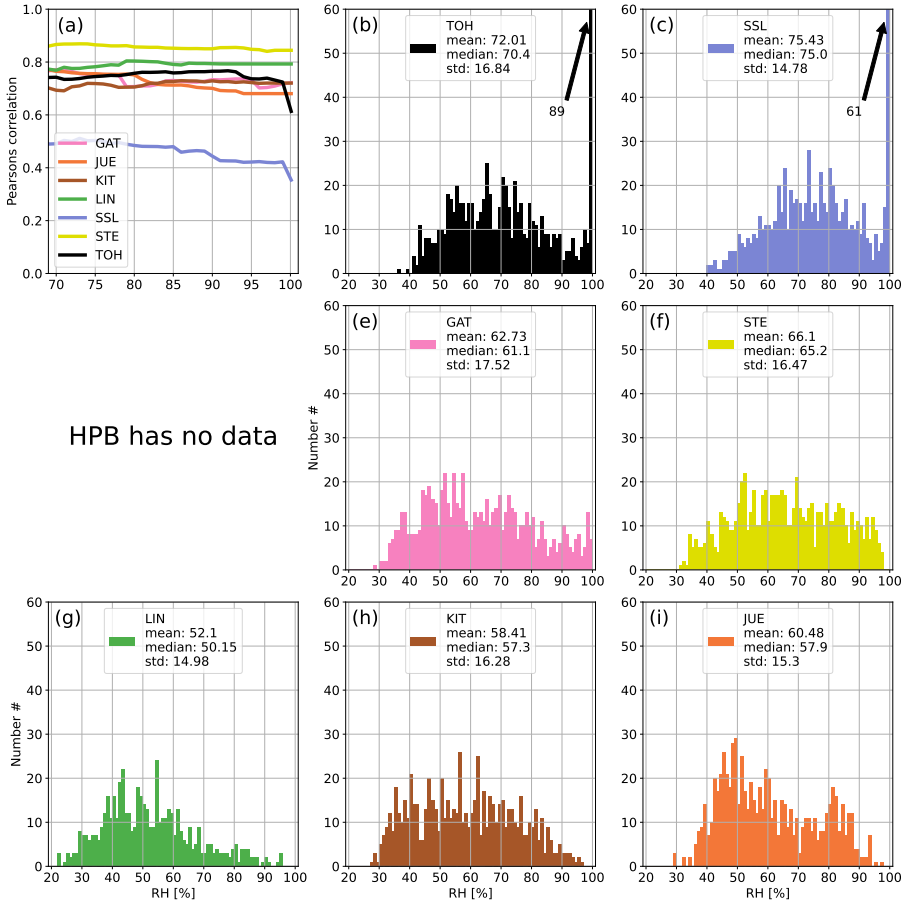

Figure A5. The panel (a) shows the development of the correlation coefficient between ^{214}Po observations and simulated ^{222}Rn data at all German ICOS stations if data with increasing RH are successively included in the calculation of the correlation. The panels (b) – (i) show the distributions of hourly RH values at the stations of the network. The arrows with numbers indicate values that exceed the y-axis range (usually for high RH). For each station the correlation coefficient was calculated only if the number of filtered data points was higher than 10% of all values for the given month to avoid the stochastic behaviour of the curves in the first subplot associated with small data sets. May 2022.

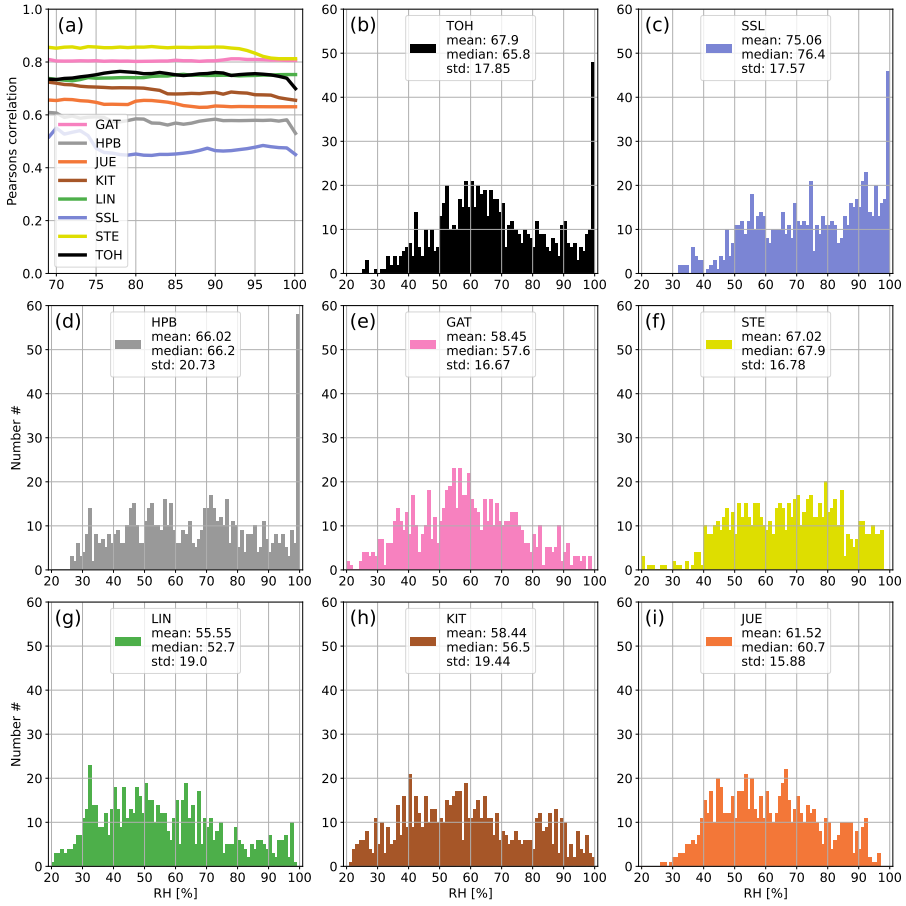

Figure A6. The panel (a) shows the development of the correlation coefficient between ^{214}Po observations and simulated ^{222}Rn data at all German ICOS stations if data with increasing RH are successively included in the calculation of the correlation. The panels (b) – (i) show the distributions of hourly RH values at the stations of the network. The arrows with numbers indicate values that exceed the y-axis range (usually for high RH). For each station the correlation coefficient was calculated only if the number of filtered data points was higher than 10% of all values for the given month to avoid the stochastic behaviour of the curves in the first subplot associated with small data sets. June 2022.

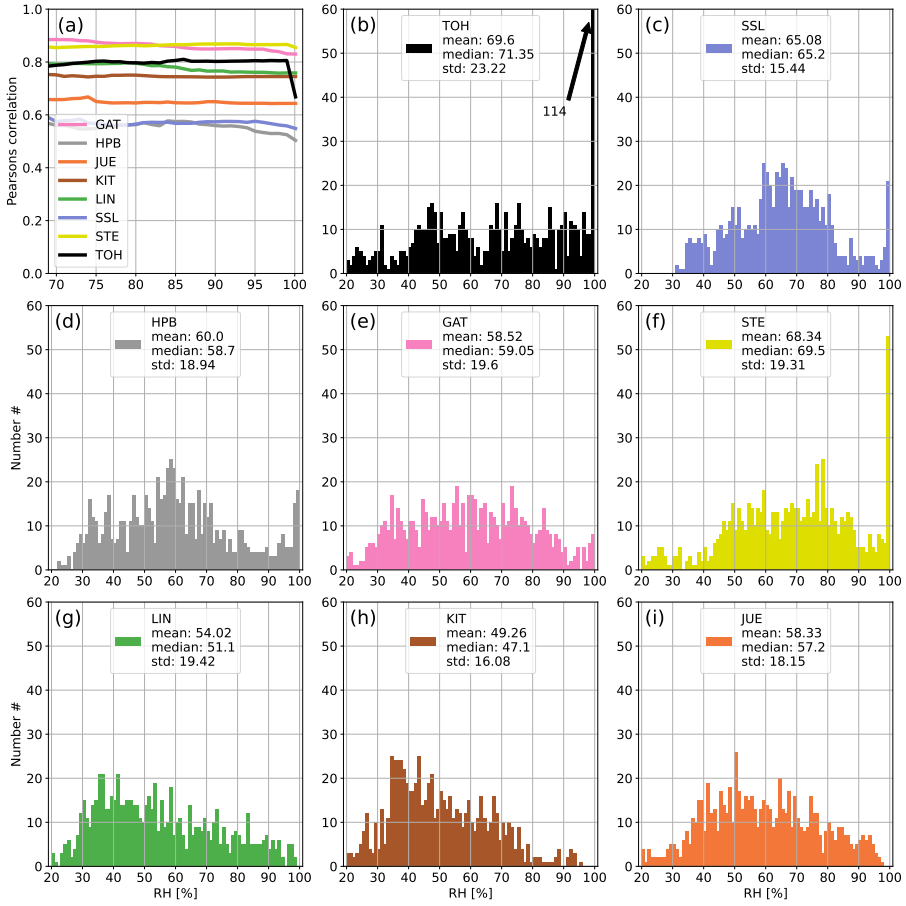

Figure A7. The panel (a) shows the development of the correlation coefficient between ^{214}Po observations and simulated ^{222}Rn data at all German ICOS stations if data with increasing RH are successively included in the calculation of the correlation. The panels (b) – (i) show the distributions of hourly RH values at the stations of the network. The arrows with numbers indicate values that exceed the y-axis range (usually for high RH). For each station the correlation coefficient was calculated only if the number of filtered data points was higher than 10% of all values for the given month to avoid the stochastic behaviour of the curves in the first subplot associated with small data sets. July 2022.

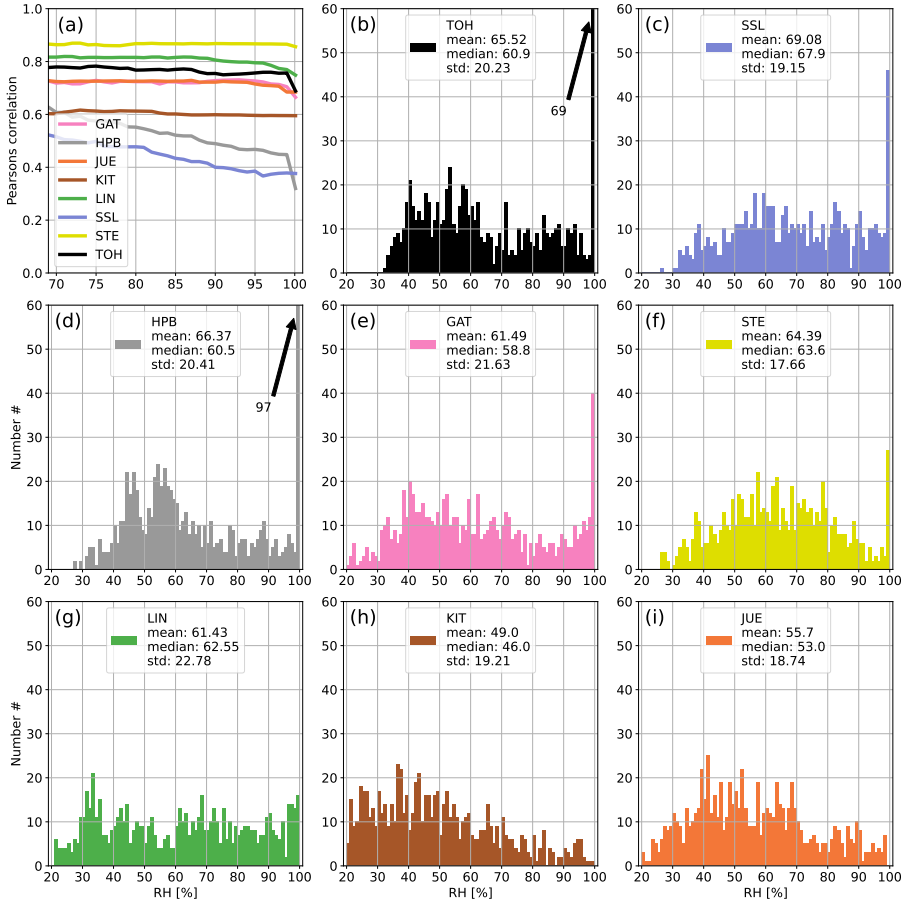

Figure A8. The panel (a) shows the development of the correlation coefficient between ^{214}Po observations and simulated ^{222}Rn data at all German ICOS stations if data with increasing RH are successively included in the calculation of the correlation. The panels (b) – (i) show the distributions of hourly RH values at the stations of the network. The arrows with numbers indicate values that exceed the y-axis range (usually for high RH). For each station the correlation coefficient was calculated only if the number of filtered data points was higher than 10% of all values for the given month to avoid the stochastic behaviour of the curves in the first subplot associated with small data sets. August 2022.

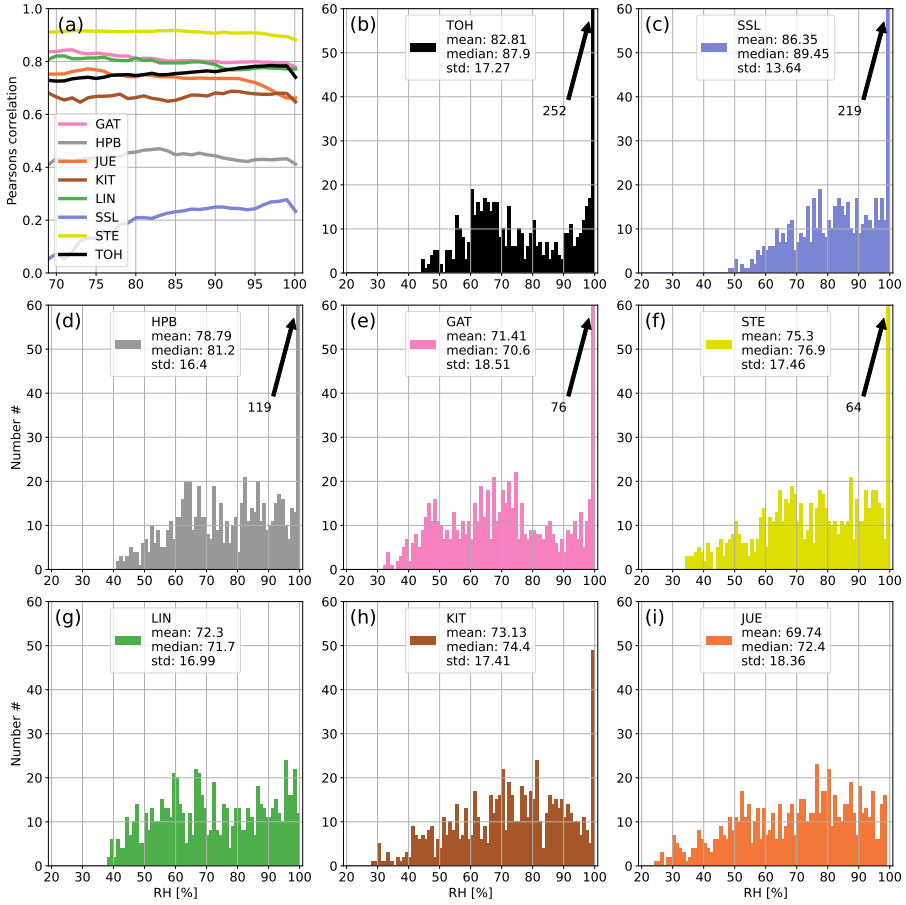

Figure A9. The panel (a) shows the development of the correlation coefficient between ^{214}Po observations and simulated ^{222}Rn data at all German ICOS stations if data with increasing RH are successively included in the calculation of the correlation. The panels (b) – (i) show the distributions of hourly RH values at the stations of the network. The arrows with numbers indicate values that exceed the y-axis range (usually for high RH). For each station the correlation coefficient was calculated only if the number of filtered data points was higher than 10% of all values for the given month to avoid the stochastic behaviour of the curves in the first subplot associated with small data sets. September 2022.

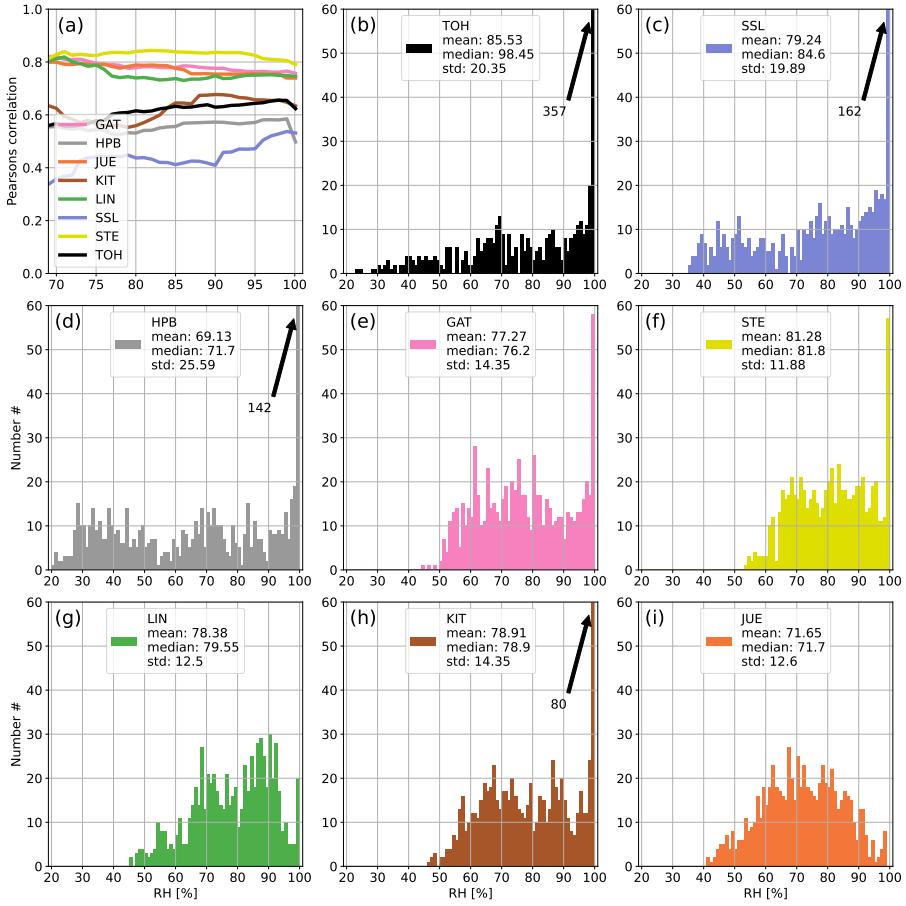

Figure A10. The panel (a) shows the development of the correlation coefficient between ^{214}Po observations and simulated ^{222}Rn data at all German ICOS stations if data with increasing RH are successively included in the calculation of the correlation. The panels (b) – (i) show the distributions of hourly RH values at the stations of the network. The arrows with numbers indicate values that exceed the y-axis range (usually for high RH). For each station the correlation coefficient was calculated only if the number of filtered data points was higher than 10% of all values for the given month to avoid the stochastic behaviour of the curves in the first subplot associated with small data sets. October 2022.

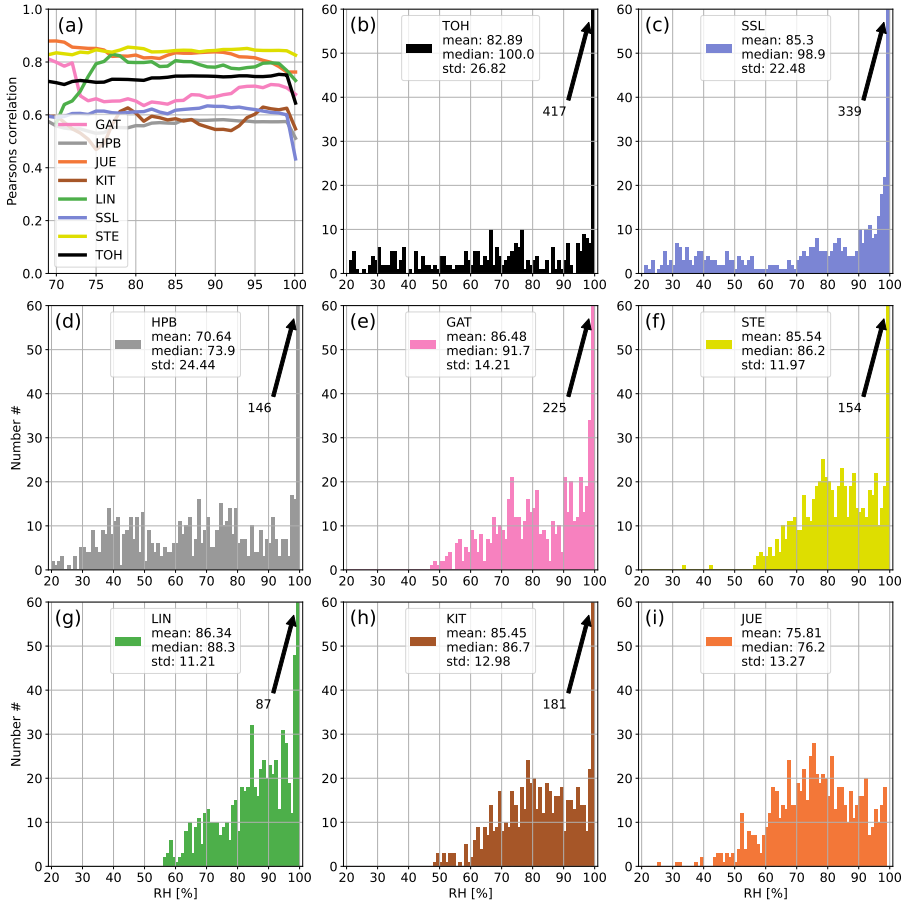

Figure A11. The panel (a) shows the development of the correlation coefficient between ^{214}Po observations and simulated ^{222}Rn data at all German ICOS stations if data with increasing RH are successively included in the calculation of the correlation. The panels (b) – (i) show the distributions of hourly RH values at the stations of the network. The arrows with numbers indicate values that exceed the y-axis range (usually for high RH). For each station the correlation coefficient was calculated only if the number of filtered data points was higher than 10% of all values for the given month to avoid the stochastic behaviour of the curves in the first subplot associated with small data sets. November 2022.

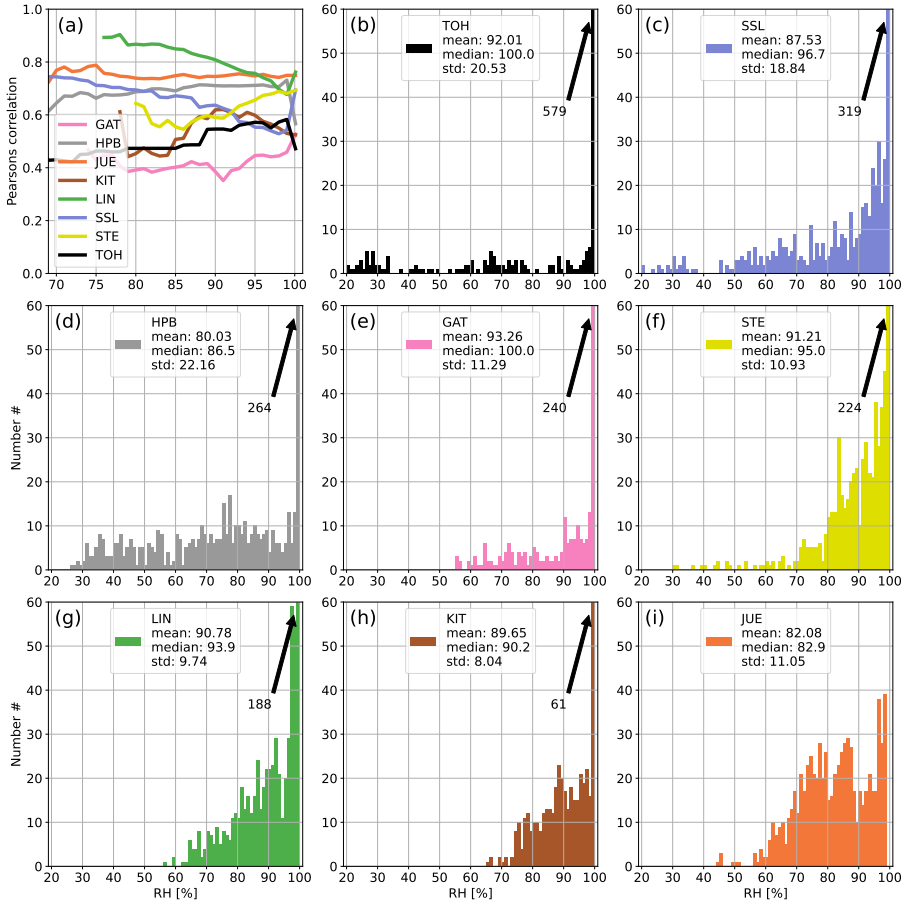

Figure A12. The panel (a) shows the development of the correlation coefficient between ^{214}Po observations and simulated ^{222}Rn data at all German ICOS stations if data with increasing RH are successively included in the calculation of the correlation. The panels (b) – (i) show the distributions of hourly RH values at the stations of the network. The arrows with numbers indicate values that exceed the y-axis range (usually for high RH). For each station the correlation coefficient was calculated only if the number of filtered data points was higher than 10% of all values for the given month to avoid the stochastic behaviour of the curves in the first subplot associated with small data sets. December 2022.

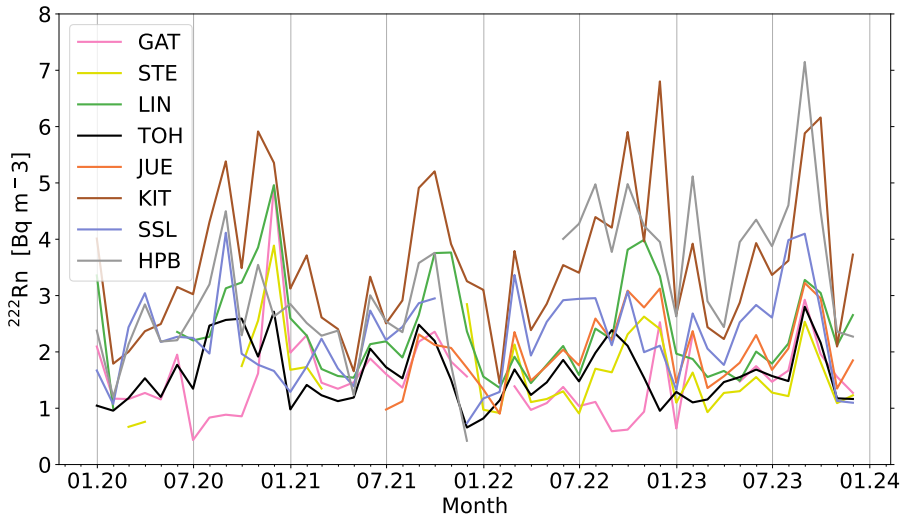

Figure A13. Seasonal cycle of ^{222}Rn monthly means at all German stations in the time period of 2020-2023. Note that monthly values are only shown if more than 70% of the daily mean values were available for the respective month.

Table 1. Parameters and locations of German ICOS stations with ^{214}Po measurements

Station	Station code (GAW ID)	Observation start	Lon (°)	Lat (°)	Station height (m a.m.s.l.)	Intake height (m a.g.l.)	Line length (m)
Gartow	GAT	November 2015	53° 04' N	11° 26' E	70	132	147
Steinkimmen	STE	October 2019	53° 03' N	08° 28' E	29	127	137
Lindenberg	LIN	February 2015	52° 10' N	14° 07' E	73	98	158
Torfhaus	TOH	April 2018	51° 49' N	10° 32' E	801	110	119
Jülich	JUE	August 2021	50° 54' N	06° 25' E	98	120	131
Karlsruhe	KIT	June 2017	49° 06' N	08° 26' E	110	100	112
Schauinsland	SSL	February 2014	47° 55' N	07° 55' E	1205	12	12
Hohenpeißenberg	HPB	October 2014	47° 48' N	11° 01' E	934	93	1